ChemComm

Accepted Manuscript

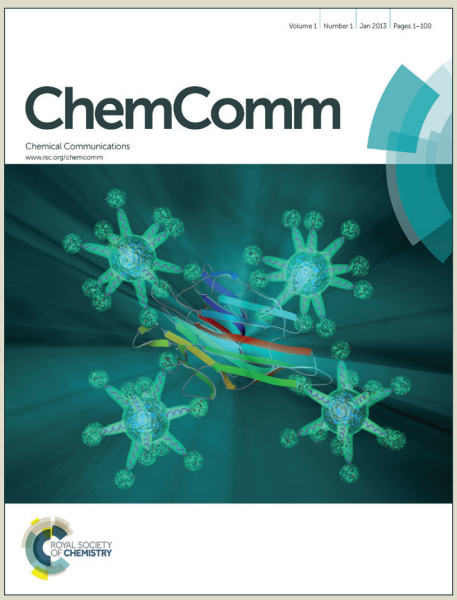

ROYAL SOCIETY OF CHEMISTRY

www.rsc.org/chemcomm

ChemComm

RSCPublishing

COMMUNICATION

A dual-emitting Cu_6-Cu_2-Cu_6 cluster as a self-calibrated, wide-range luminescent molecular thermometer†

Cite this: DOI: 10.1039/x0xx00000x

Jun-Hao Wang, Mian Li, Ji Zheng, Xiao-Chun Huang* and Dan Li*

Received 00th January 2014
Accepted 00th January 2014

DOI: 10.1039/x0xx00000x

www.rsc.org/chemcomm

A tetradecanuclear copper(I) cluster compound, namely $[Cu_6L_3(Cu_2I_2)Cu_6L_3]$ (H_2L = 3,5-bis((3,5-dimethyl-pyrazol-4-yl)methyl)-2,6-dimethylpyridine), is synthesized. The high thermal stability, well-resolved blue/red dual emissions and two-way luminescent thermochromism warrant its self-calibrated temperature sensing ability, covering a wide range (120–450 K). These promising results are supported by combined structural, spectral and computational studies.

Materials that show luminochromism responding to temperature variation have attracted interdisciplinary interest because of their potential as luminescent molecular thermometers (LMTs) and merits of intrinsic visual read-out and non-contact measurement.[1-3] In principle, the read-out signals, i.e. the responses of emission spectra, can be the vertical (intensity) or horizontal (wavelength) changes or the combination of both. Remarkably, dual-emitting systems can overcome the limitation of intensity-based temperature sensors by providing self-calibrated (aka. ratiometric) signals, or by admitting visual emission colorimetric responses.[2,3] However, most dual-emitting temperature sensors that are actively sought are those with nanostructures,[3a] which lack designability from the molecular level. Recently, a few ratiometric LMTs based on lanthanide compounds were reported.[2]

In comparison, luminescent transition metal complexes[4] often possess long lifetimes, visible-range absorption, moderate brightness, and large Stokes shifts. These features are favorable for LMTs; however, surprisingly, only a few well investigated mononuclear, unitary (i.e. with only one emissive excited centre) metal complexes were utilized as intensity-based LMTs.[1a,5] There are only two known cases of cluster-based LMTs,[6] which usually have multiple emissive excited states suitable for the generation of dual emissions. A recently reported Cu_5 cluster that functioned as a LMT did show luminescent thermochromism in the range of 228–353 K, but the multiple excited states experienced thermal equilibration and thus no dual emission was observed, and therefore Cu_5 is only an intensity- and lifetime-based LMT.[6a] The classical Cu_4I_4 phosphor was able to exhibit dual bands, making self-calibration possible. However, the additional band only occurred under cryogenic conditions, and hence the ratiometric Cu_4I_4 LMT was only applicable in the range of 8–120 K.[6b]

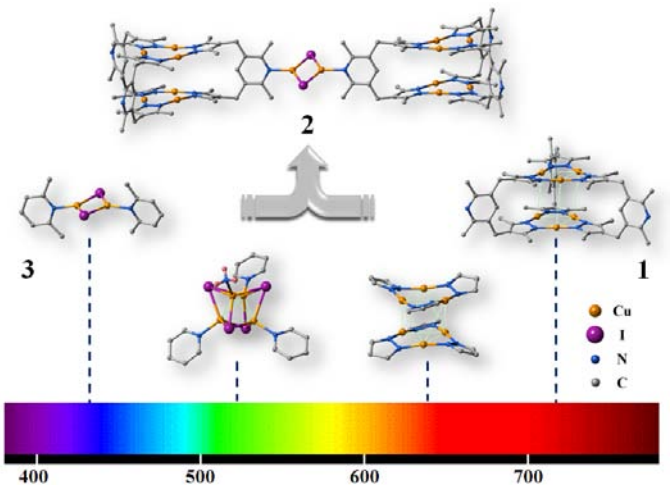

Fig. 1 The emission colour profiles of four copper(I) cluster-based phosphors, Cu_2I_2, Cu_4I_4, $[Cu_3Pz_3]_2$ and Cu_6Pz_6 (from left to right) in the visual spectrum, and the binary compound (upper) uniting the Cu_2I_2 and Cu_6Pz_6 clusters. C–H bonds are omitted here.

Our group has been interested in cluster-based phosphors and their thermochromic properties,[7] especially for copper(I)-halide[7a-c,8] and copper(I)-pyrazolate[7d-f,9] clusters. Aiming at producing self-calibrated, wide-range cluster-based LMTs, one must tackle the following difficulties: i) that of maintaining the stability of materials at elevated temperature; ii) that of resolving dual emissions in one matrix and within a wide temperature

range; iii) that of avoiding quenched intensity and lifetime under higher temperature due to increasing nonradiative transition rate.[10] Although the well known Cu_4I_4[7a-c,8] and Cu_3Pz_3[7d-f,9] (Pz = pyrazolate) clusters are capable of retaining their characteristic emissions in one matrix, their emission peaks (λ^{em}_{max1} 520–550 nm for Cu_4I_4; λ^{em}_{max2} 630–660 nm for $[Cu_3Pz_3]_2$) are too close (Fig. 1), leading to an overlap of the dual bands.[7b,c] Such a complex photophysical scheme is unfavorable for self-calibrated LMTs.

Here we demonstrate the fabrication of an advanced binary copper(I) cluster-based dual emitter, namely $[Cu_6\mathbf{L}_3(Cu_2I_2)Cu_6\mathbf{L}_3]$ (denoted **2**, $H_2\mathbf{L}$ = 3,5-bis((3,5-dimethyl-pyrazol-4-yl)methyl)-2,6-dimethylpyridine; $Cu_6\mathbf{L}_3$ denoted **1**, Cu_2I_2(2,6-lutidine)$_2$ denoted **3**) and its utilization as a self-calibrated, wide-range LMT. As shown in Fig. 1, the well-resolved dual emissions are assured by selecting two other copper(I) cluster phosphors whose emission peaks lie at either end of the visual spectrum. The prototype of the red phosphor, a Cu_6Pz_6 cage compound,[7d] benefits from its unusual stacking mode which is responsible for the huge Stokes shift (λ^{em}_{max2} 710 nm, compared with that of $[Cu_3Pz_3]_2$). For the blue phosphor, we note that blue-emitting Cu_4I_4 cluster is not yet reported, but blue emission is available for the Cu_2I_2 type.[11,12] The organic linker in this study is thus modified to 2,6-lutidine-like: the pyridine-N site is left for further coordination with CuI, and the 2,6-dimethyl provides steric hindrance to prevent the formation of the bulkier Cu_4I_4.

The binary cluster **2** is synthesized through a stepwise procedure: by first reacting the new ligand $H_2\mathbf{L}$ with Cu_2O to afford the crystalline product **1**; then the bulk sample of **1** is introduced to further react with CuI to give the final product **2** (see Experimental Section in ESI†). The variation of reactant ratio (CuI:**1**) does not change the final product, and the direct reaction of CuI and $H_2\mathbf{L}$ cannot yield **2**. The isolated cluster **3** can be readily synthesized for the comparison of luminescence. The crystal structures of **1**, **2** and **3** (shown in Fig. 1) are demonstrated by single-crystal X-ray diffraction (see Crystal Data Section in ESI†), and the purity of all samples for luminescence measurements are confirmed by elemental analysis and powder X-ray diffraction (Fig. S2 in ESI†).

The intertrimeric Cu^I-Cu^I contacts within the cages, which are the origin of the red emission, have slightly longer distances for **1** (shortest 4.04 Å) and **2** (shortest 3.83 Å) relative to those of Cu_6Pz_6 cage (shortest 3.69 Å[7d]) at 298 K (Fig. S1 in ESI†). These distances are shortened (shortest 3.74 Å) at 100 K, revealed by the cryogenic structure of **2**. Temperature-varied powder X-ray diffraction of **2** indicates no phase transition occurs under high temperature (298–573 K, Fig. S2c in ESI†), consistent with thermogravimetric analysis which reveals the thermal decomposition temperature is up to 660 K for **2** (Fig. S3 in ESI †). Such a high thermal stability is the prerequisite for fabricating a wide-range LMT, with which the above difficulty i) is tackled.

To ensure the spectral characteristics of Cu_6Pz_6 and Cu_2I_2 are well preserved in the tetradecanuclear cluster **2** (i.e. tackling ii)), the absorption, excitation and emission spectra and decay lifetimes of **1**, **2** and **3** are studied in detail (see Physical Measurement Section in ESI†; selected spectral profiles are given in Table 1). The hypothesis of well-resolved, wide-temperature-range dual emissions is convinced by the following spectral evidences:

1) The dual bands of **2** with λ^{em}_{max1} and λ^{em}_{max2} well correspond with those of **3** and **1**, respectively.
2) The excitations λ^{ex}_{max} of **2** monitored at λ^{em}_{max1} and λ^{em}_{max2} also coincide exactly with those of **3** and **1**, respectively.
3) The phosphorescence lifetimes of the dual bands of **2** are close to those of separated **1** and **3**, and the trends of shorter lifetimes under elevated temperature are similar. The microsecond-scale lifetimes, although shortened due to nonradiative transition, suggest the triplet excited states are not fully quenched under high temperature up to 450 K (thus tackling difficulty iii)).
4) Most importantly, the characteristic gradual red shift of **1** (due to the shortened Cu^I-Cu^I contacts, see also Fig. S18 in ESI†) upon lowering temperature is also observed in the varying λ^{em}_{max2} of **2** excited at 290 nm and ranging from 450→100 K (also consistent with the above observation in the crystal structure of **2** at 100 K).

Table 1. Luminescence profiles of **1-3** from 100→450 K.

Compounds	λ^{ex}_{max} (nm)	λ^{ex}_{max} (nm)	τ (μs) [e]
1	290→300 [a]	740→685 [b]	9.58→5.48 [b]
2	293→310 [a]	1: 420 2: 740→695 [b]	13.27→5.35 [b]
	310, 340 [c]	1: 420 [d] 2: 740→690	17.21→5.10 [d]
3	310, 340 [c]	420, 440 [d]	16.25→6.56 [d]

[a] monitored at 740 nm emission; [b] excited at 290 nm; [c] monitored at 420 nm emission; [d] excited at 337 nm; [e] decay lifetime of the major emission (see Table S3 in ESI†). Note "→" indicates the trends upon varying temperature.

For visual temperature monitor, the bulk samples of **2** exhibit an interesting two-way luminescent thermochromism (Fig. 2a): under 254 nm UV lamp the emission colour varies from magenta to dark red responding to the high-temperature range, while 365 nm UV light exposure gives the varying colours from blue to purple. Both cases are reversible when switching back to 298 K. The distinct responses are believed to originate from the different excitation energies of Cu_6Pz_6 and Cu_2I_2, and hence temperature-varied emission spectra of LMT **2** excited at 290 (Fig. 2b), 310 (Fig. 2c) and 340 nm (Fig. S8c in ESI†) are recorded.

The colour changes correspond well with the variation of the relative emission intensity (I_1:I_2) of λ^{em}_{max1}:λ^{em}_{max2} upon varying temperature. For example, at 290 nm excitation which is optimal for the red-emitting Cu_6Pz_6 cluster, the emission intensity at λ^{em}_{max2} is comparable with that of λ^{em}_{max1}, showing colours from magenta (the mix of red and blue) to red corresponding to 100–450 K (Fig. 2b). In contrast, at 310 and 340 nm excitations, the λ^{em}_{max2} intensity is significantly lower, giving blue to purple colours, which are mainly attributed to the blue-emitting Cu_2I_2 cluster. Interestingly, when excited at 310 nm, although the expected blue shift of λ^{em}_{max2} upon increasing temperature is observed, the intensity first raises and then drops (Fig. 2c), contradicting to general photophysical observation.[4] Such a

phenomenon is also observed for the isolated Cu_6Pz_6 cluster **1** excited at 310 nm (Fig. S6 in ESI†), indicating there is a thermal activation process for the functioning of the Cu_6Pz_6 excimer when prompted under non-optimal excitations.[7d-f,9]

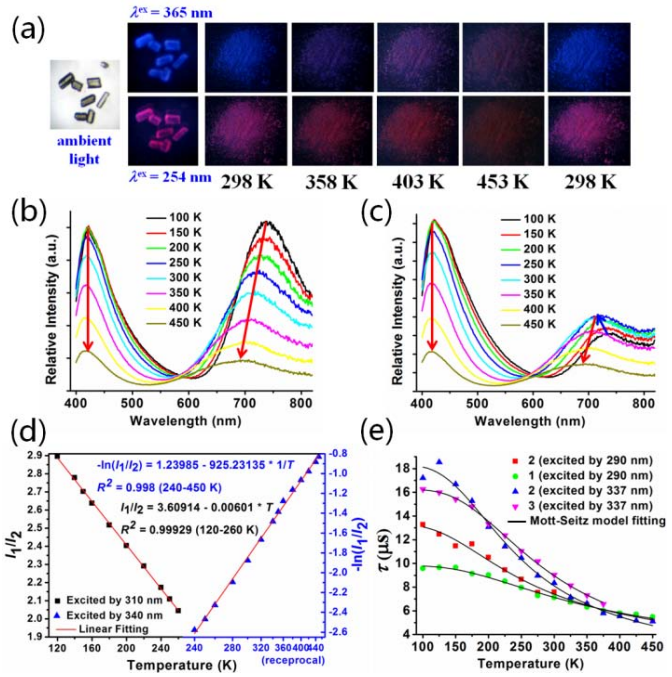

Fig. 2 (a) Visual temperature monitor of **2** under UV lamp with different λ^{ex}. Temperature-varied emission spectra excited at (b) 290 nm and (c) 310 nm, respectively. The arrows indicate the intensity changes at λ^{em}_{max}. (d) Working curves and equations ($I_1/I_2 \sim T$) of the ratiometric LMT **2** implemented at 310 (black) and 340 nm (blue, reciprocal coordinate) excitations. (e) Temperature dependence of the emission decay lifetimes of **1**-**3** and the best fit using the Mott-Seitz model ($R^2 > 0.989$).

To assess the self-calibrated performance of **2**, we measure the emission spectra with a narrower temperature interval (20 K, Fig. S11 in ESI†), and correlate temperature (T) to the emission intensity ratio I_1:I_2 (Fig. S12-S14 in ESI†).[1,2] Linear correlations can be found in two segments: 120–260 K for λ^{ex} = 310 nm (sensitivity 0.208–0.285 % K^{-1}) and 240–450 K for λ^{ex} = 340 nm (sensitivity 0.283–0.088 % K^{-1}, Fig. S19 in ESI†).[1,2f] The working curves and equations ($I_1/I_2 \sim T$) of **2** are given in Fig. 2d. The working principle of this dual-emitting system involves a thermally activated nonradiative process, demonstrated by the fitted Arrhenius-like (Mott-Seitz model, see Fig. S15 in ESI†)[2a,e,6a] decay lifetimes (Fig. 2e). The thermal activation energies are calculated to be 4.96±0.35 (**2**, λ^{ex} = 290 nm), 5.98±0.36 (**1**, λ^{ex} = 290 nm), 6.12±0.36 (**2**, λ^{ex} = 337 nm) and 7.01±0.19 (**3**, λ^{ex} = 337 nm) kJ mol^{-1}, respectively.

To gain a better interpretation of the photophysical process of **2** from the quantum level, we perform preliminary DFT and TDDFT calculations (Fig. 3; see Computational Section in ESI†). The results and analysis are summarized as follows:

1) The typical highest occupied molecular orbitals (HOMOs) and lowest unoccupied molecular orbitals (LUMOs) of **1** and **3** are, as expected, well preserved in **2** (HOMO and LUMO of **2** correspond to HOMO and LUMO of **3**; HOMO-3/-4 and LUMO+2/+3 of **2** correspond to HOMO and LUMO of **1**), demonstrated by the similarity of both the orbital contours and the quantitative descriptions of orbital compositions (Table S4 and S5 in ESI†).
2) The energy levels and HOMO-LUMO gap of **1** are very close to the counterparts in **2**, while both the energy levels of HOMO and LUMO of **3** raise a bit for the counterparts in **2** and the HOMO-LUMO gap is larger for **2**, indicating the union of the Cu_2I_2 and Cu_6Pz_6 clusters slightly alters the electronic structure in the binary system. But the origins of the two major excited states of **2** are largely unaltered, being metal/halide-to-ligand charge transfer (for λ^{em}_{max1} band) and cluster-centered transition (for λ^{em}_{max2} band).
3) Interestingly, the major spin-allowed absorption transitions (Table S6-S8 in ESI†) of **1** (largest oscillator strength f = 0.019) are much weaker than those of **3** (largest f = 0.11), but a notable inter-cluster transition (f = 0.16, green arrow in Fig. 3) can efficiently populates the Cu_6Pz_6-related excited states in **2**. This inter-cluster transition may be responsible for the shoulders (*ca.* 350 nm) in the experimental excitation spectra of **2** (Fig. S7b in ESI†), which is unobserved in those of **1** (Fig. S5 in ESI†). The existence of inter-cluster transition implies the possibility of electron/energy transfer cannot be ruled out, but there is no direct evidence for the process of thermally activated energy transfer, especially considering the lifetime profiles (Fig. 2e) in which **1**-**3** undergo similar thermal deactivation process.
4) The low oscillator strengths of **1**, indicating nearly forbidden radiative decay,[6a] are consistent with the spectral observation of first-raising-then-dropping emission intensity at λ^{em}_{max} of **1** excited at non-optimal wavelengths (Fig. S6 in ESI†), which is also responsible for the unusual excitation-energy-dependent two-way luminescent thermochromism of **2**.

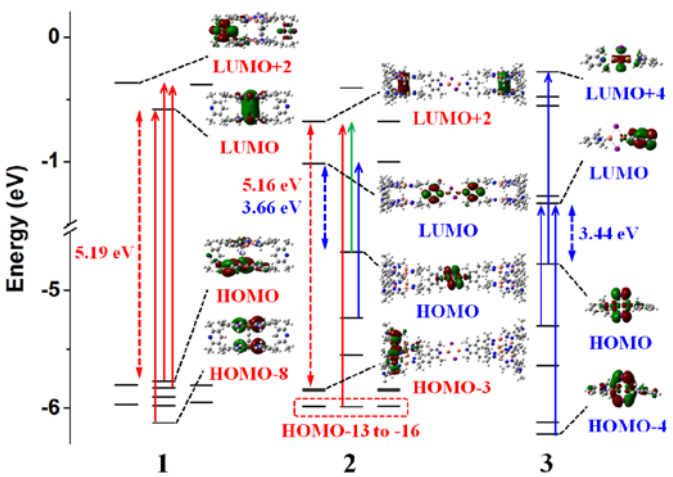

Fig. 3 Summary of calculated frontier molecular orbitals, energy levels and gaps, and major excitation transitions of **1**-**3**. The contours of orbitals are selected from Fig. S16 in ESI†. The two-side arrows with dashed lines show the HOMO-LUMO gaps of **1** and **3** and their counterparts in **2**. The one-side arrows with solid lines show the major excitation transitions selected from Table S6-S8 in ESI†. The

red and blue arrows represent the intra-cluster transitions related to Cu_6Pz_6 and Cu_2I_2, respectively, while the green one is a considerable inter-cluster transition from HOMO to LUMO+3 of **2**.

In conclusion, a dual-emitting molecular photofunctional entity incorporating two types of copper(I) clusters, Cu_2I_2 and Cu_6Pz_6, is designed and synthesized. The well retained and resolved dual emissions of both cluster components provide the basis for the implementation of this binary system as a self-calibrated LMT. This tetradecanuclear copper(I) cluster represents a novel LMT featuring the highest nuclearity and the widest sensing range for LMTs to date (120–450 K), which is fundamentally different from the well-developed, but more expensive lanthanide-based LMTs. Moreover, the combined structural, spectral and computational studies on this binary cluster (**2**) and its isolated counterparts (**1** and **3**) would shed light on a better understanding of the structure-property relationship of dual-emitting system in general photochemistry.

This work was supported by the National Basic Research Program of China (nos. 2012CB821706 and 2013CB834803), and the National Natural Science Foundation of China (nos. 21171114 and 91222202). The authors wish to thank Dr. Chensheng Ma for the discussion on photophysical property, and Mr. Tian Lu for the discussion on orbital composition analysis.

Notes and references

Department of Chemistry and Key Laboratory for Preparation and Application of Ordered Structural Materials of Guangdong Province, Shantou University, Guangdong 515063, P. R. China. E-mail: xchuang@stu.edu.cn; dli@stu.edu.cn

† Electronic Supplementary Information (ESI) available: experimental details, crystal data (CCDC 949368-949371 and 983600), physical measurements and computational details. See DOI: 10.1039/c000000x/

1 For reviews on temperature sensors and LMTs: (a) X.-d. Wang, O. S. Wolfbeis and R. J. Meier, *Chem. Soc. Rev.*, 2013, **42**, 7834; (b) M. Schäferling, *Angew. Chem. Int. Ed.*, 2012, **51**, 3532; (c) S. Uchiyama, A. P. de Silva and K. Iwai, *J. Chem. Edu.*, 2006, **83**, 720.

2 For lanthanide-based dual-emitting LMTs: (a) C. D. S. Brites, P. P. Lima, N. J. O. Silva, A. Millán, V. S. Amaral, F. Palacio and L. D. Carlos, *Adv. Mater.*, 2010, **22**, 4499; (b) Y. Cui, H. Xu, Y. Yue, Z. Guo, J. Yu, Z. Chen, J. Gao, Y. Yang, G. Qian and B. Chen, *J. Am. Chem. Soc.*, 2012, **134**, 3979; (c) X. Rao, T. Song, J. Gao, Y. Cui, Y. Yang, C. Wu, B. Chen and G. Qian, *J. Am. Chem. Soc.*, 2013, **135**, 15559; (d) Y. Cui, W. Zou, J. Yu, W. Zhang, Y. Yang and G. Qian, *Chem. Commun.*, 2014, **50**, 719; (e) K. Miyata, Y. Konno, T. Nakanishi, A. Kobayashi, M. Kato, K. Fushimi and Y. Hasegawa, *Angew. Chem. Int. Ed.*, 2013, **52**, 6413; (f) A. Cadiau, C. D. S. Brites, P. M. F. J. Costa, R. A. S. Ferreira, J. Rocha and L. D. Carlos, *ACS Nano*, 2013, **7**, 7213.

3 For other dual-emitting temperature sensors: (a) E. J. McLaurin, L. R. Bradshaw and D. R. Gamelin, *Chem. Mater.*, 2013, **25**, 1283, references therein; (b) N. Chandrasekharan and L. A. Kelly, *J. Am. Chem. Soc.*, 2001, **123**, 9898; (c) G. A. Baker, S. N. Baker and T. M. McCleskey, *Chem. Commun.*, 2003, 2932.

4 For reviews on general photochemistry of transition metal complexes: (a) S.-W. Lai and C.-M. Che, *Top. Curr. Chem.*, 2004, **241**, 27 (Pt); (b) S. Campagna, F. Puntoriero, F. Nastasi, G. Bergamini and V. Balzani, *Top. Curr. Chem.*, 2007, **280**, 117 (Ru); (c) Y. Chi and P.-T. Chou, *Chem. Soc. Rev.*, 2010, **39**, 638 (Ir); (d) V. W.-W. Yam and E. C.-C. Cheng, *Chem. Soc. Rev.*, 2008, **37**, 1806 (Au); (e) N. Armaroli, G. Accorsi, F. Cardinali and A. Listorti, *Top. Curr. Chem.*, 2007, **280**, 69 (Cu).

5 For examples: (a) J. Stehr, J. M. Lupton, M. Reufer, G. Raschke, T. A. Klar and J. Feldmann, *Adv. Mater.*, 2004, **16**, 2170 (Pt); (b) S. M. Borisov, A. S. Vasylevska, C. Krause and O. S. Wolfbeis, *Adv. Funct. Mater.*, 2006, **16**, 1536 (Ru); (c) L. H. Fischer, M. I. J. Stich, O. S. Wolfbeis, N. Tian, E. Holder and M. Schäferling, *Chem. Eur. J.*, 2009, **15**, 10857 (Ir).

6 (a) D. Cauzzi, R. Pattacini, M. Delferro, F. Dini, C. Di Natale, R. Paolesse, S. Bonacchi, M. Montalti, N. Zaccheroni, M. Calvaresi, F. Zerbetto and L. Prodi, *Angew. Chem. Int. Ed.*, 2012, **51**, 9662; (b) C. Tard, S. Perruchas, S. Maron, X. F. Le Goff, F. Guillen, A. Garcia, J. Vigneron, A. Etcheberry, T. Gacoin and J.-P. Boilot, *Chem. Mater.*, 2008, **20**, 7010.

7 (a) R. Peng, M. Li and D. Li, *Coord. Chem. Rev.*, 2010, **254**, 1; (b) S.-Z. Zhan, M. Li, X.-P. Zhou, J.-H. Wang, J.-R. Yang and D. Li, *Chem. Commun.*, 2011, **47**, 12441; (c) S.-Z. Zhan, M. Li, S. W. Ng and D. Li, *Chem. Eur. J.*, 2013, **19**, 10217; (d) G.-F. Gao, M. Li, S.-Z. Zhan, Z. Lv, G.-h. Chen and D. Li, *Chem. Eur. J.*, 2011, **17**, 4113; (e) J.-H. Wang, M. Li and D. Li, *Chem. Sci.*, 2013, **4**, 1793; (f) W.-X. Ni, M. Li, J. Zheng, S.-Z. Zhan, Y.-M. Qiu, S. W. Ng and D. Li, *Angew. Chem. Int. Ed.*, 2013, **52**, 13472.

8 (a) P. C. Ford, E. Cariati and J. Bourassa, *Chem. Rev.*, 1999, **99**, 3625; (b) S. Perruchas, X. F. Le Goff, S. Maron, I. Maurin, F. Guillen, A. Garcia, T. Gacoin and J.-P. Boilot, *J. Am. Chem. Soc.*, 2010, **132**, 10967; (c) X.-c. Shan, F.-l. Jiang, D.-q. Yuan, H.-b. Zhang, M.-y. Wu, L. Chen, J. Wei, S.-q. Zhang, J. Pan and M.-c. Hong, *Chem. Sci.*, 2013, **4**, 1484.

9 (a) H. V. R. Dias, H. V. K. Diyabalanage, M. G. Eldabaja, O. Elbjeirami, M. A. Rawashdeh-Omary and M. A. Omary, *J. Am. Chem. Soc.*, 2005, **127**, 7489; (b) J.-P. Zhang, S. Horike and S. Kitagawa, *Angew. Chem. Int. Ed.*, 2007, **46**, 889; (c) T. Jozak, Y. Sun, Y. Schmitt, S. Lebedkin, M. Kappes, M. Gerhards and W. R. Thiel, *Chem. Eur. J.*, 2011, **17**, 3384; (d) A. C. Jahnke, K. Pröpper, C. Bronner, J. Teichgräber, S. Dechert, M. John, O. S. Wenger and F. Meyer, *J. Am. Chem. Soc.*, 2012, **134**, 2938.

10 (a) S. L. Shinde and K. K. Nanda, *Angew. Chem. Int. Ed.*, 2013, **52**, 11325; (b) N. B. Shustova, A. F. Cozzolino, S. Reineke, M. Baldo and M. Dincă, *J. Am. Chem. Soc.*, 2013, **135**, 13326.

11 (a) H. Araki, K. Tsuge, Y. Sasaki, S. Ishizaka and N. Kitamura, *Inorg. Chem.*, 2005, **44**, 9667; (b) D. M. Zink, M. Bächle, T. Baumann, M. Nieger, M. Kiihn, C. Wang, W. Klopper, U. Monkowius, T. Hofbeck, H. Yersin and S. Bräse, *Inorg. Chem.*, 2013, **52**, 2292.

12 (a) J. A. Campbell, C. L. Raston and A. H. White, *Aust. J. Chem.*, 1977, **30**, 1937; (b) P. C. Healy, J. D. Kildea, B. W. Skelton and A. H. White, *Aust. J. Chem.*, 1989, **42**, 115.

Graphical abstract

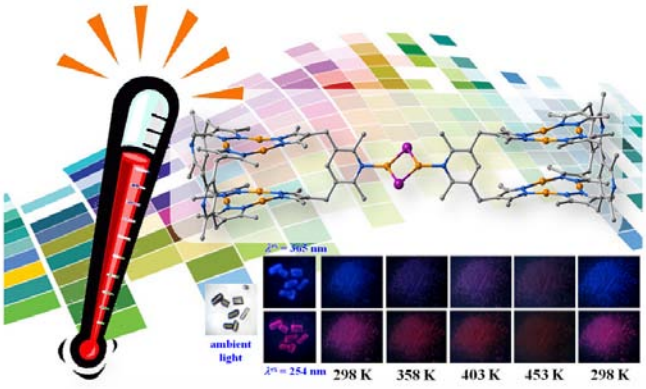

The union of two red-emitting cage-like clusters, Cu_6Pz_6 (Pz = pyrazolate), joined by a blue-emitting Cu_2I_2 cluster, allows the internally referenced temperature sensing within a wide range (120–450 K).